Chapter 8

Results

This section deals with the results from the optimization design studies performed using the design methodology for the 2-D, side view, MAGLEV vehicles in ground effect. We first discuss the 5 design variable problem which turns out to be flawed due to a non-smooth design space. A higher dimensional problem with 7 design variables is then developed to combat the deficiency in the original formulation. Optimizations are then performed, using the 7 design variable problem for several objective functions. The designs and their attributes are discussed and compared to those from Northrop Grumman which were used as baseline designs for this study.

The 5 design variable problem uses the 5 geometry variables outlined in Fig. 7.1 and two constraints. The first constraint requires XF to be greater than XN, and the second constraint requires the drag coefficient to be positive, as discussed in Chapter 7. An optimization was performed using the Northrop Grumman MAG1007 as a baseline design. The SQP optimizer never hones in on an optimum point during the computation time allotted. This is due to the non-smooth design space which causes the SQP algorithm to take steps through the design space based on bad gradient information. Non-smooth design space is typical of real engineering problems and is a major obstacle in engineering design optimization. The bumps in the design space stem from the analyses of flow over bluff bodies. Small, continuous changes in the geometry definition variables can produce discontinuous values for the aerodynamic coefficients. This is mainly a result of movement of the separation points.

Figure 8.1 is a plot of the optimization with the MAG1007 baseline and drag coefficient as the objective function. The abscissa shows the design space index which steps one for every SQP iteration. This index does not indicate the search direction in the 5 dimensional space, nor does it indicate the length of each step. The total length traveled from the baseline to iteration number 15 is 3.41. The direct distance between the two points is 2.2. The optimization path is shown as a solid line with boxes indicating the discrete steps taken by the optimizer.

To illustrate the problem with the 5 design variable formulation, we can take a closer look at iteration number 12. The distance along the search direction from iteration 12 to iteration 13 is 0.0452. The step along this search direction results in a higher objective function. The actual design space along this step in the 5 dimensional search direction is shown with a dashed line. The section shown here is constructed using 20 evenly spaced steps along the search direction for a length twice that of the optimization step. The non-smooth nature of the design space is apparent. Using the gradient information obtained by finite differencing at iteration 12, along with the approximation for the Hessian of the Lagrangian, a quadratic model of the Lagrangian is formed. The quadratic model of the Lagrangian is shown in Fig. 8.1 as the dashed/dotted line. Based on the gradient information at iteration 12 as well as the build up of gradient information from passed iterations in the approximation to the Hessian, the optimizer thinks it is stepping in a direction which lowers the Lagrangian. There are no active constraints during this optimization, so a lowered Lagrangian should correspond to a lower objective function. Due to the violation of the smoothness requirement the quadratic subproblems are not representative of the actual design space in the region of the iteration.

In order to combat this deficiency with this formulation of the problem, it was instead reposed as a 7 design variable optimization. The two additional design variables are the locations of the top and bottom surface separation points. The aerodynamic forces are functions of the vehicle shape and the flow conditions (the 5 design variables and the Reynolds number). More exactly, the geometry and the free stream flow conditions determines the separation locations, and therefore the circulation, which determines the forces on the vehicle which are the integrated pressure and skin

friction over the surface.

According to this new formulation, these two separation locations are independent variables and not functions of the 5 original design variables as they once were. As independent variables they will most probably not match their correct value according to their functional dependence on the other variables and flow parameters. So, we are solving for flows in which the separation locations do not match the pressure field in hopes that this projected design space is smoother than that in 5 dimensions. Two equality constraints are then imposed which require each separation location to match the pressure field; the Stratford Criterion is imposed as a constraint [71]. Each equality constraint is enforced using two inequality constraints so this formulation adds four new constraints to the SQP problem. Optimization theory requires that the solution be feasible at the optimum point but allows for infeasible iteration steps along the way. The idea of projecting the design space in such a manner as to smooth out the design space was developed during personal conversations with Dr. Eugene Cliff. This formulation utilizes a seventh constraint which requires the flow to remain attached until reaching the aft end of the vehicle thereby avoiding designs which cannot be handled by the boundary layer calculation.

One problem associated with the implementation of this idea is that the objective function is a much stronger function of the separation locations than of the 5 geometry variables. If left as is, this formulation of the problem will result in optimizations requiring many SQP iterations. The separation locations which are strong variables will be changed much more than the geometry variables which are weak variables. Affine scaling is used to prevent this. This scaling is aimed at producing equal changes in the objective function for equal changes in each of the scaled design variables. Equation 8.1 shows the functional form of the scaling.

$$\mathbf{x} = \mathbf{NOM} + \mathrm{SCALE} \times \mathbf{Z} \tag{8.1}$$

The unscaled design variables, $\mathbf{x}$, are sent to the analyses while the scaled design variables, $\mathbf{Z}$, are sent to the optimizer. The ranges of the scaled design variables go from approximately 0.0 to 1.0 for the range of interest in the corresponding unscaled variables. The matrix, SCALE, is a diagonal matrix with the diagonal elements

corresponding to the value of the derivative of $\mathbf{x}$ with respect to $\mathbf{Z}$ that makes the coefficient of the linear term of the Taylor Series expansion of the objective function with respect to the scaled variables a constant (Eq. 8.2).

$$\begin{aligned} \text{OBJ} &= f(\mathbf{x}) \\ \text{OBJ} - \text{OBJ}_o &= \sum_{i=1}^{n} \frac{\partial f}{\partial Z_i} \Delta Z_i + \ldots \\ &= \sum_{i=1}^{n} \frac{\partial f}{\partial x_i} \frac{\partial x_i}{\partial Z_i} \Delta Z_i + \ldots \\ &= \sum_{i=1}^{n} \frac{\partial f}{\partial x_i} \text{SCALE}_i \Delta Z_i + \ldots \\ \frac{\partial f}{\partial x_i} \text{SCALE}_i &= \text{Constant for all i} \end{aligned} \tag{8.2}$$

Figure 8.2 shows the optimization path through the design space using this 7 design variable formulation. It is an equivalent plot to that shown in Fig. 8.1 for the 5 dimensional case. Again, we are looking at iteration number 12. The dark boxes indicate that the iteration step is at an infeasible point in the design space. The scaled length of the step in the search direction between iteration steps 12 and 13 is 0.5110. The objective function along this search direction in 7 dimensional space is shown as the dashed line for twice the length of the iteration step. The design space is much smoother than its 5 dimensional counterpart and will, therefore, be more conducive for finite differencing derivatives. The quadratic model of the Lagrangian along the search direction is shown in the dashed/dotted line. The quadratic model of the Lagrangian increases as does the objective function. Both iteration 12 and 13 are infeasible points, so there is at least one active constraint included in the Lagrangian. The quadratic model is developed using better gradient information and does a better job following the design space. The optimization is successfully completed after 18 iterations. The total length traveled through the design space from the baseline to the optimum point is 7.82, and the straight line distance between the two points in the 7 dimensional space is 0.50. The 7 design variable formulation has provided a projected design space which is navigable by calculus-based optimizers.

Another benefit of the 7 design variable formulation is that the CPU time required per analysis is reduced to approximately 1.5 minutes, down from 6.5 minutes on a

Silicon Graphics Power Challenge with an R8000 processor chip. By prescribing the separation locations and not letting them develop over time, the transient from the impulsive start is approximately 50 time steps shorter. Since the CPU time is approximately proportional to the square of the number of time steps, any reduction in the number of time steps taken will greatly shorten the computational time.

The 7 design variable formulation does have a drawback. The non-smooth design space was replaced with a smooth one and highly convex equality constraints. The two inequality constraints, forming the top separation point equality constraint, are prohibitive in finding a global optimum point. Figure 8.3 shows a set of analyses between two optimum drag coefficient points. The first point was arrived at from a MAG950 baseline design while the second point was arrived at from a MAG1007 baseline. The search direction is a straight line from one point to the other in 7 dimensional space. The dotted line shows the equality constraint tolerance. Any constraint value within ± 0.03 is considered to be satisfied. The values of the constraints for the top and bottom separation points are shown in the dashed line. The top separation point constraint is highly convex and is violated for most of the space between these two optima along the straight path between the two points. The highly convex equality constraints result in a design space with many isolated, local optima i.e. a 7 dimensional "egg crate." Different starting points in the design space will lead to different optimum points. The two optimum points based on drag coefficient have objective functions with nearly the same magnitude (Fig. 8.3). In order to use this method as a design tool, one must optimize several times from different positions in the design space and make an engineering decision as to which design to accept. This is essential for the optimization problem here due to the nature of the design space and is good practice for any problem, since there is no mathematical proof for the convergence to a global optimum point. Improvements to this method might involve the development of another formulation which can provide the differentiable objective function without the inclusion of convex equality constraints.

Optimizations are performed for the objective functions of drag coefficient, lift to drag ratio, empty weight, vehicle cost, operating cost, and life cycle cost. All of these optimizations employ the 7 design variable problem formulation. The aerodynamic

analyses are performed for full-scale vehicles.

8.1 Optimum Drag Coefficient Designs

The optimizations for drag coefficient as the objective function were run from two different baselines - MAG950 and MAG1007. Figure 8.4 shows the baseline, MAG950, and the optimized drag coefficient design derived from it. The drag coefficient was reduced from 0.2025 to 0.0489. This 75.9% reduction is due to a 95.4% reduction in the base drag and a 1.43% reduction in the skin friction drag. The pressure coefficient plots for the the baseline and optimum points for this design are shown in Fig. 8.5.

Figure 8.6 shows the baseline, MAG1007, and the optimized drag coefficient design derived from it. This design is referred to as the OPTCD2 design and the MAG950 baseline design is referred to as the OPTCD1 design based solely on the order that the calculations were performed. This optimization results in an optimum point different from that of the OPTCD1 design. The drag coefficient is reduced from 0.1984 to 0.0424. This 78.6% reduction in the drag coefficient is due to a 99.2% reduction in the base drag and a 4.4% reduction in the skin friction drag. The pressure coefficient plots for the the baseline and optimum points for this design are shown in Fig. 8.7. The "blips" in the pressure coefficient profiles for the optimum designs are due to the panel spacing and quantity which are not adjusted during the optimization. Figure 8.8 shows the OPTCD2 pressure coefficient as calculated during the optimization and after the surface grid is refined. Improvements to this methodology might include automatic grid refinements during the optimization process.

Figure 8.9 shows a comparison of both optimum drag coefficient designs. The optimizations from the two different baseline designs resulted in two local optima with roughly the same objective function value. Both optimum designs are more blunt than their baselines and yet they achieve minimum drag coefficients. These designs exploit the ground effect phenomena to greatly reduce the base drag. As part of the lift reversal phenomena, the upstream stagnation point is pulled down to a lower position. A blunt nose quickly expands the flow producing a leading edge suction which offsets the base drag caused by flow separation. Figures 8.10 and

8.11 show the two minimum drag coefficient designs along with top surface pressure profiles for in and out of ground effect flow. The respective stagnation point locations are indicated. It is apparent that for ground effect flow these designs provide a large amount of expansion around the leading edge of the vehicle. The leading edge suction here may be slightly augmented due to the aerodynamics model. We can recall the calculations performed for the flow over an elliptic cylinder in ground effect (Fig. 2.31) where the vortex method predicts a larger shift in the attachment and separation point locations than is predicted using a Navier-Stokes CFD code.

For a point of comparison a design optimization was performed to minimize the drag coefficient while assuming an out of ground effect aerodynamic condition. This was performed to show the difference in the aerodynamics problem and the need to design specifically for ground effect flow. The optimization was performed from the MAG950 baseline. Figure 8.12 shows the baseline and the optimum design. This design shows a side view which is very close to being symmetric top to bottom. The asymmetric geometry definition prevents this from occurring. The drag coefficient for the out of ground effect flow was reduced from 0.1472 to 0.0510. The pressure coefficient plot in Fig. 8.13 shows the optimum drag coefficient design with higher base pressure than that of the baseline. In contrast to this design, the ground effect designs have a drooped nose and a blunt top surface used for the quick expansion of the top surface flow. The ground effect drag coefficient for this design is 0.1529, so the use of out of ground effect analyses for the design of ground effect vehicles is not advised.

Figure 8.14 shows a comparison of the two minimum drag coefficient designs to the five 2-D, side view designs from Northrop Grumman. All of these designs were evaluated based on drag coefficient as a figure of merit. The optimum designs are both blunt and resemble the Northrop Grumman MAG1459. As calculated here by the vortex panel method, the MAG1459 is the lowest drag coefficient design proposed by Northrop Grumman. As was calculated using a Navier-Stokes CFD code [28], the MAG1459 had the second lowest drag coefficient.

These optimizations resulted in changes to the other figures of merit which we are dealing with via separate optimizations. Both optimum drag coefficient designs

resulted in vehicles with slightly higher weight and, therefore, higher vehicle cost due to the weight engineering model. Due to the lower drag coefficients, both designs resulted in much lower operating costs and, therefore, lower life cycle cost. These designs will be compared to the designs based on the other figures of merit in a quantitative fashion in Section 8.6.

8.2 Maximum Lift to Drag Ratio Designs

Next, optimizations were performed to maximize the lift to drag ratio, because this ratio traditionally plays a major role in determining the efficiency and performance of aerospace vehicles. A high lift to drag ratio design can possibly lead to lower direct operating cost since less energy would be required to provide magnetic levitation and propulsion. Since optimizations are usually formulated in terms of a minimization problem this one was set up to minimize the ratio of drag to lift. For these calculations, four baselines are used; the MAG950, MAG1007, and the two minimum drag coefficient designs - OPTCD1 and OPTCD2. The optimization for the baseline MAG1007 resulted in an infeasible solution, so it is not shown here. The results of the other three optimizations are shown in Fig. 8.15. The solid lines represent the baseline designs and the dashed lines represent the optimum designs. The design from the MAG950 baseline results in a 63.9% increase in the lift to drag ratio from its baseline value of 17.09 to the optimum value of 28.01. The design from the OPTCD1 drag coefficient optimum baseline results in an assumed convergence due to a null search direction on the first iteration. The OPTCD1 drag coefficient optimum is also a local optimum point for the lift to drag ratio at a value of 68.03. The greatest value for lift to drag ratio was achieved with the OPTCD2 optimized drag coefficient point as a baseline. The lift to drag ratio was increased marginally from 83.33 to 84.75. This final design provides the greatest objective function found among the sampled local optima. It will be used in Section 8.6 as the design for maximum lift to drag ratio even though we have no mathematical proof that this design point is the global optimum point. A bar chart of the normalized lift to drag ratio can be seen in Fig. 8.16.

8.3 Optimum Operating Cost Designs

Optimizations for minimizing the operating cost were then performed for four baseline designs; the MAG950, MAG1007, and the two minimum drag coefficient designs - OPTCD1 and OPTCD2. The objective function is scaled due to the large magnitude of its values.

$$\text{OBJ} = \frac{|\text{Operating Cost}|}{1.0E^8} \tag{8.3}$$

The absolute value of the operating cost is taken, since its value is usually taken to be negative.

The four baseline designs and their resulting optima can be seen in Fig. 8.17. The solid lines represent the baseline designs and the dashed lines represent the optimum designs. The design based on the MAG950 baseline is similar to the corresponding design for lift to drag ratio in Fig. 8.15, and it actually has a higher lift to drag ratio (44.05). This is what provides the lower operating cost, since less energy is expended to lift and propel the vehicle. The maximum lift to drag ratio design does not exactly correspond to the minimum operating cost design, since the propulsion and levitation systems operate at different efficiencies and energy consumptions. In addition to this, the maximum lift to drag ratio design can have higher drag. The design from the MAG1007 baseline resulted in a 33.6% reduction in the operating costs. The design from the OPTCD1 optimized drag coefficient baseline results in an assumed convergence due to a null search direction on the first iteration. The lowest value for the operating cost resulted from the OPTCD2 optimized drag coefficient design baseline. The optimization takes one step to an infeasible design with a slightly higher objective function. The design is shown in Fig. 8.17 even though it is not feasible.

Figure 8.18 shows the normalized operating cost for the four optimizations discussed here. The MAG950 operating cost is used to normalize all of the values. It can be seen that all of the optimum points have similar values for the objective function. Due to the highly convex equality constraints in the design space, we are forced to make decisions concerning the best designs based on the completion of several calculations to find local optima. The lowest operating cost among these calculations is for the OPTCD2 optimized drag coefficient baseline design. This design will therefore

be used as the minimum operating cost design for the comparisons in Section 8.6.

8.4 Optimum Acquisition Cost Designs

Optimizations were performed to minimize the acquisition cost from the four baseline designs; the MAG950, MAG1007, and two optimized drag coefficient designs - OPTCD1 and OPTCD2. A scaled objective function is used due to the large magnitude of the acquisition cost.

$$\text{OBJ} = \frac{\text{Acquisition Cost}}{1.0E^7} \tag{8.4}$$

This acquisition cost is the cost of a single vehicle. The total investment cost is calculated as part of the life cycle cost calculation. The vehicle cost is directly proportional to the vehicle weight, so the minimum cost vehicle is also the minimum weight vehicle. These were presented previously as two separate figures of merit but are discussed here together due to the models used. According to the weight model, the minimum weight vehicle will have the minimum surface area, or length for a 2-D design. The design from the baseline MAG1007 in Fig. 8.19 provides the minimum acquisition cost, since it has the minimum surface length. The top and bottom surfaces of the nose are practically straight lines which gives the least surface length. This design provides a 0.08% reduction in the acquisition cost due to the 0.10% reduction in empty weight. The total range of vehicle weights is very small, and so, due to the weight engineering model, the vehicle cost is very insensitive to the design variables. This problem is discussed further in Chapter 4.

The minimum acquisition cost design provides minor improvements at the price of penalties in operating cost and life cycle cost. These penalties result from the poor aerodynamics of this minimum acquisition cost design ($C_D = 0.2305$). The operating cost increases by 4.3% and the life cycle cost increases by 0.8% (both increases are from nonoptimal values). Figure 8.19 also shows designs from the MAG950 and optimized drag coefficient design baselines. The MAG950 and optimized drag coefficient OPTCD1 baseline designs result in assumed convergence due to a null search direction on the first SQP iteration. The optimized drag coefficient OPTCD2 baseline

design moves slightly to reduce the vehicle cost by less than 0.005%. A bar chart of the normalized acquisition cost, referred to the MAG950 acquisition cost, for the four optimizations performed can be seen in Fig. 8.20. The ordinate ranges from 0.98 to 1.00, so the reader can detect the small differences in acquisition cost among the designs.

8.5 Optimum Life Cycle Cost Designs

Finally, life cycle cost optimizations were performed with a scaled objective function due to the large magnitudes of the life cycle cost.

$$\text{OBJ} = \frac{|\text{Life Cycle Cost}|}{1.0E^9} \tag{8.5}$$

The optimizations were performed from four baseline designs; the MAG950, MAG1007, and the two optimized drag coefficient designs - OPTCD1 and OPTCD2. The baselines and their respective optima can be seen in Fig. 8.21. The solid line represents the baseline and the dashed line represents the optimum design. Both of the optimized drag coefficient baseline designs resulted in null search directions and are, therefore, also local minimum life cycle designs. The optimization from the MAG950 baseline resulted in a 6.9% reduction in the life cycle cost and the optimization from the MAG1007 baseline resulted in a 7.1% reduction in the life cycle cost. All of the local optima have similar values of the objective function. This can be seen in Fig. 8.22 which shows the normalized life cycle cost for the four optimizations performed. The normalization was performed using the life cycle cost for the MAG950. The relatively small reduction in the life cycle cost (less than 10%) is due to the insensitive acquisition cost model. Improvements to this model will allow us to tap into a large component of the life cycle cost. The minimum life cycle cost design is that from the optimized drag coefficient design, OPTCD2.

8.6 Comparison of Designs for Various Figures of Merit

In the previous sections of this chapter, a single design was chosen from each to represent the optimum design for that figure of merit. In this section, these designs are compared to gain insight into the design problem and the workings of the MDO design methodology. Each of these optimum designs is not necessarily a global optimum point, since there is no way to prove convergence to such a point. In addition to this, the highly convex equality constraints precludes searching for a global optimum point.

The bar charts in Fig. 8.23 and 8.24 show a comparison of the designs based on different figures of merit. The designs are shown on the abscissa and are identified by the objective function optimized for each one. The optimum designs for the drag coefficient, operating cost, and life cycle cost are the same design. The maximum lift to drag ratio design is one arrived at from optimizing the minimum drag coefficient design to minimize the ratio of drag to lift. The minimum acquisition cost design is one arrived at by optimizing from the MAG1007 baseline. The MAG950 and MAG1007 baseline designs are also shown.

The drag coefficient for each of the optimized designs is shown at the top of Fig. 8.23. The optimum acquisition cost design has the highest drag coefficient, followed by the two baseline designs. The optimum drag coefficient, direct operating cost, and life cycle cost designs are the same design, and they, therefore, have the same attributes. These designs have nearly the same drag coefficient as the optimum lift to drag ratio design which has a marginally higher drag coefficient.

Also shown in Fig. 8.23 is a plot of the lift to drag ratio for the different designs. The lowest values of the lift to drag ratio are obtained by the baseline designs and the optimum acquisition cost design. The optimum lift to drag ratio design has a marginally greater ratio than the design with optimum drag coefficient, direct operating cost, and life cycle cost.

A plot of normalized direct operating cost can be seen at the top of Fig 8.24. The values are normalized using the MAG950, so it has a normalized cost of unity.

The baseline designs and the optimum acquisition cost design have the highest direct operating cost due their poor aerodynamic performance. The remaining designs have similar values for the direct operating cost. The optimized lift to drag ratio design actually has a slightly lower operating cost than the optimum operating cost design. Results such as this are entirely possible due to the convex equality constraints in the design space.

Figure 8.24 also shows plots for the acquisition cost and the life cycle cost, at the middle and the bottom. Both of these plots are normalized using the MAG950 values. The plot of normalized acquisition cost shows the ordinate from 0.980 to slightly higher than unity. This is done so that the reader can detect the slight differences in vehicle cost among the designs. The optimum acquisition cost design has a marginally lower acquisition cost. The optimum life cycle cost design shows a slightly less than 10.0% reduction in the life cycle cost. The optimum lift to drag ratio design has a slightly lower life cycle cost than the optimum life cycle cost design. This is due to the lower operating cost experienced by this design. The difference in the life cycle cost between these designs in indistinguishable on this plot and is almost certainly within the uncertainty on these cost models. Greater variation in designs and sensitivity to the design variables can be achieved with the use of a more advanced acquisition cost model. Table 8.1 shows the geometry variables for all of the optimum designs.

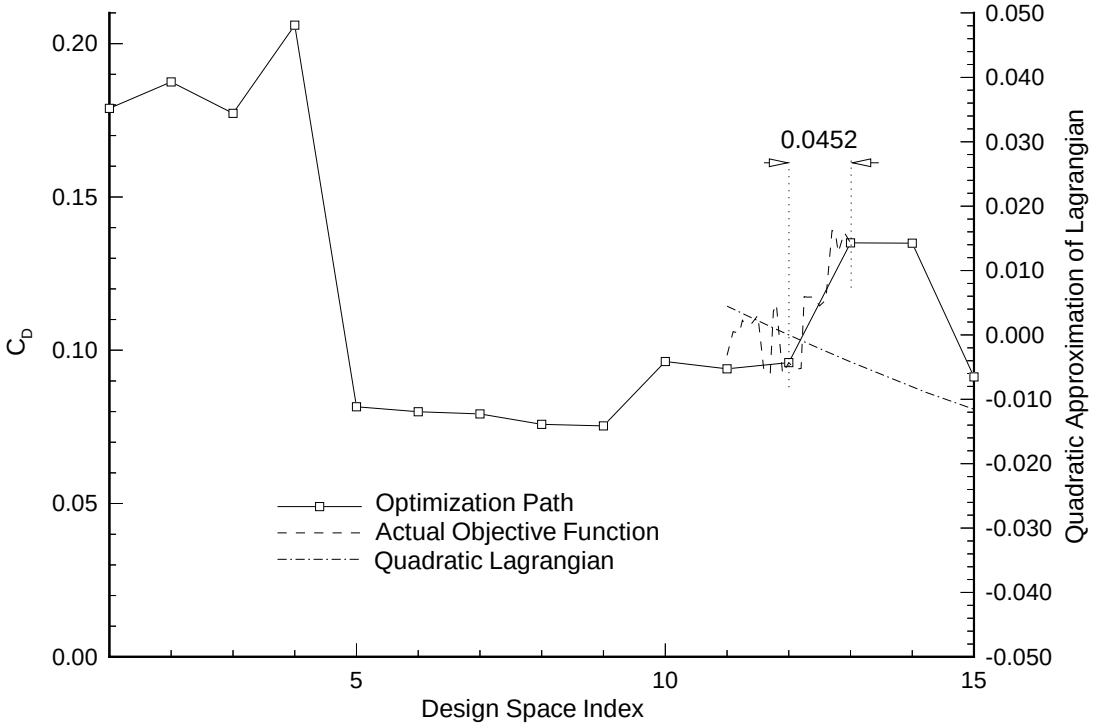

Figure 8.1: 5 Design Variable Optimization for Drag Coefficient

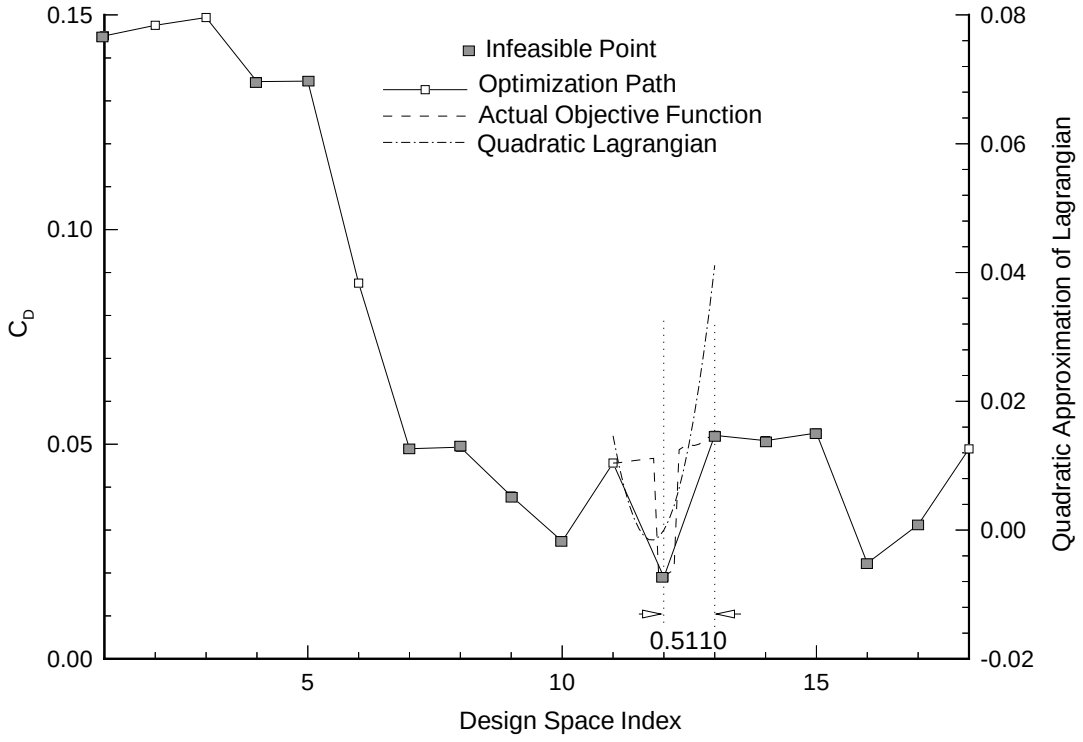

Figure 8.2: 7 Design Variable Optimization for Drag Coefficient

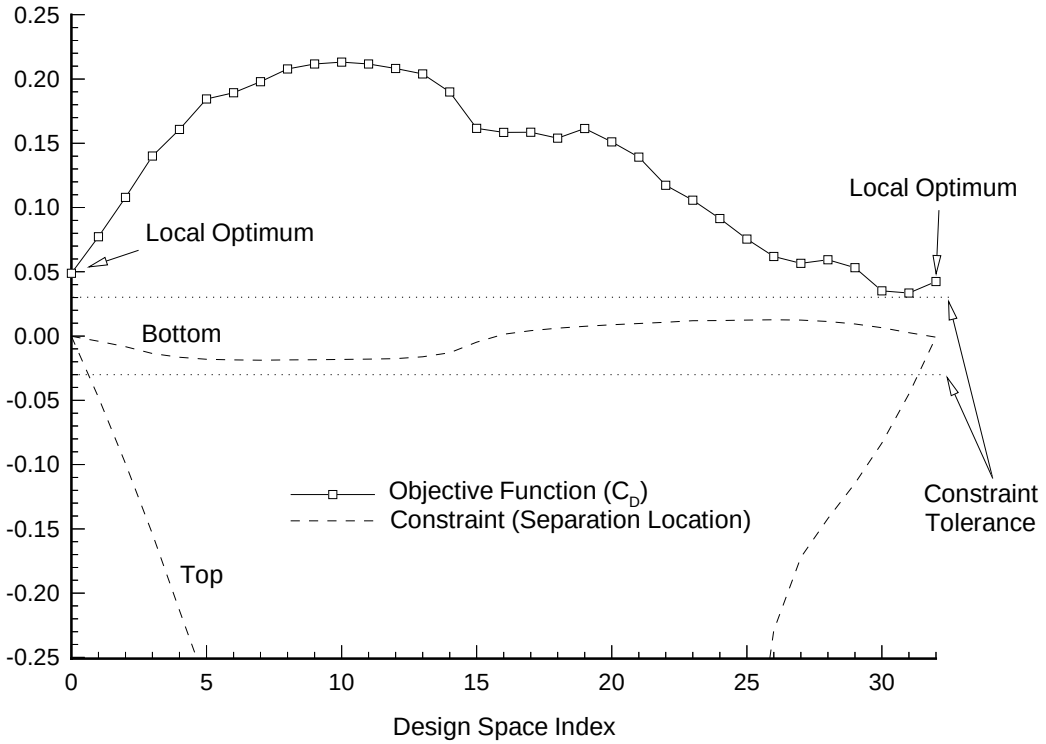

Figure 8.3: Design Space Between Local Drag Coefficient Optima; MAG950 at the Left End and MAG1007 at the Right End

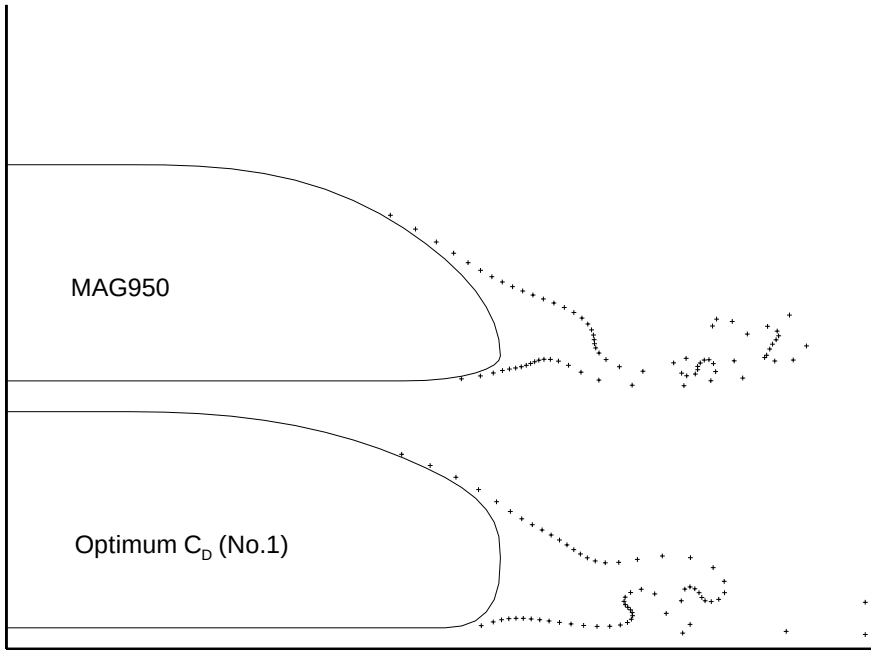

Figure 8.4: Optimum Drag Coefficient Design Using MAG950 Baseline

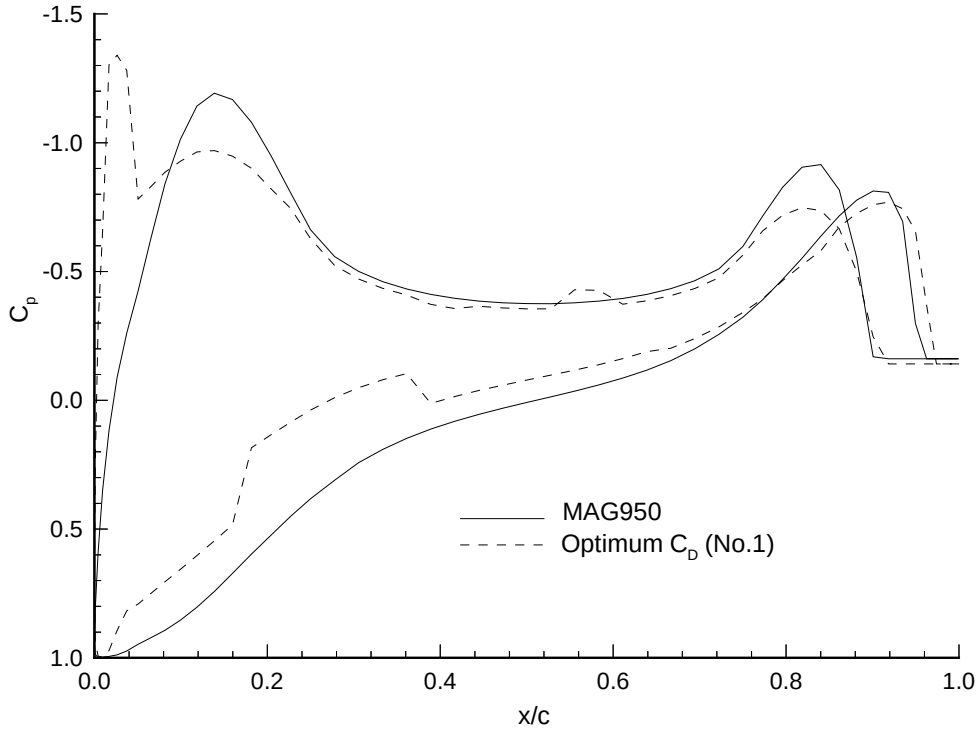

Figure 8.5: Pressure Coefficients for Optimum Drag Coefficient Design Compared to MAG950 Baseline

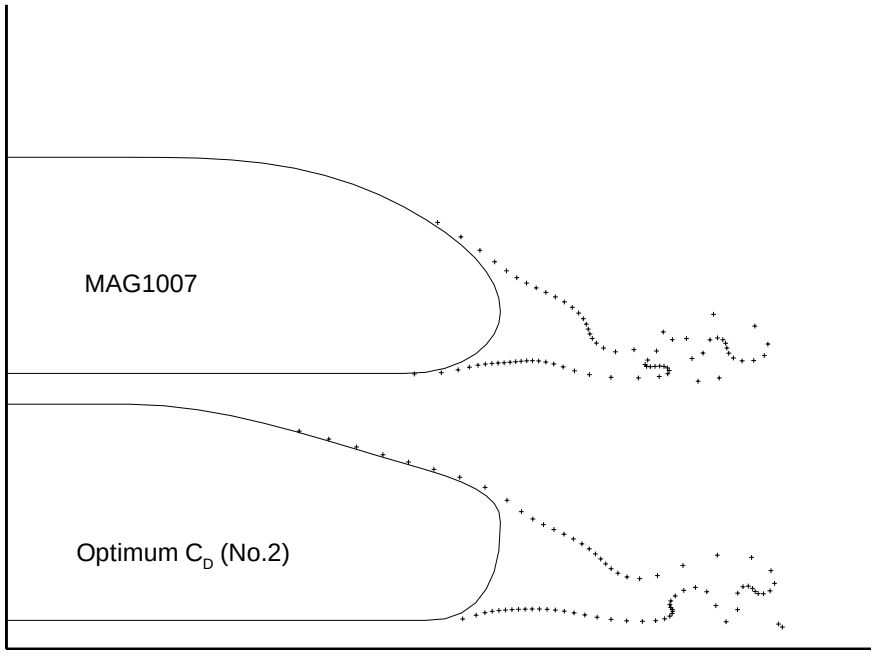

Figure 8.6: Optimum Drag Coefficient Design Using MAG1007 Baseline

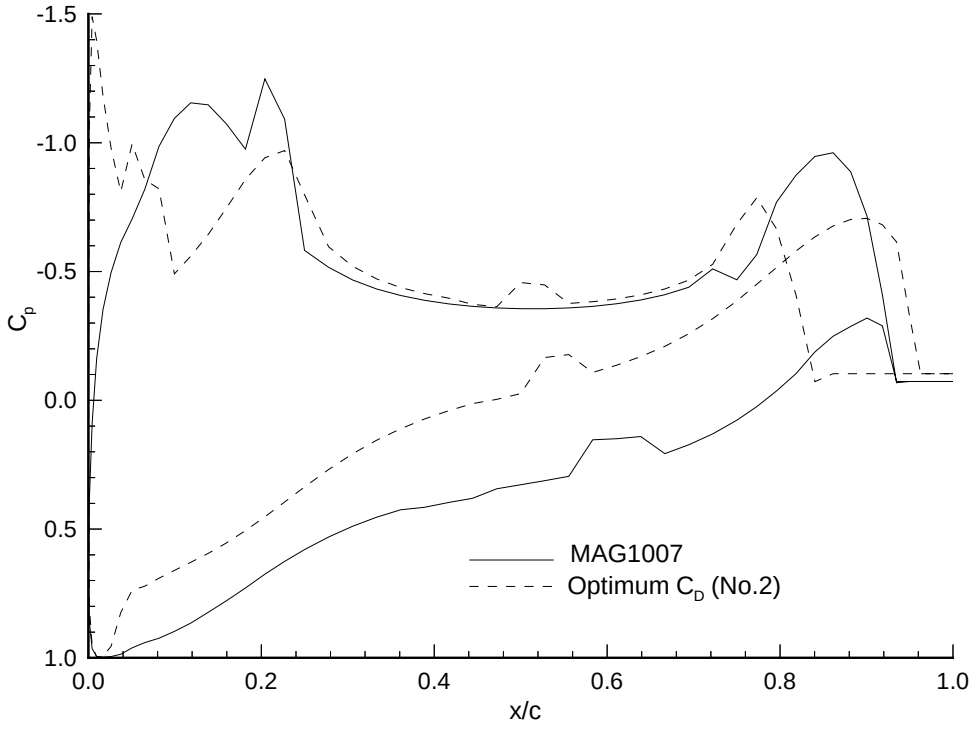

Figure 8.7: Pressure Coefficients for Optimum Drag Coefficient Design Compared to MAG1007 Baseline

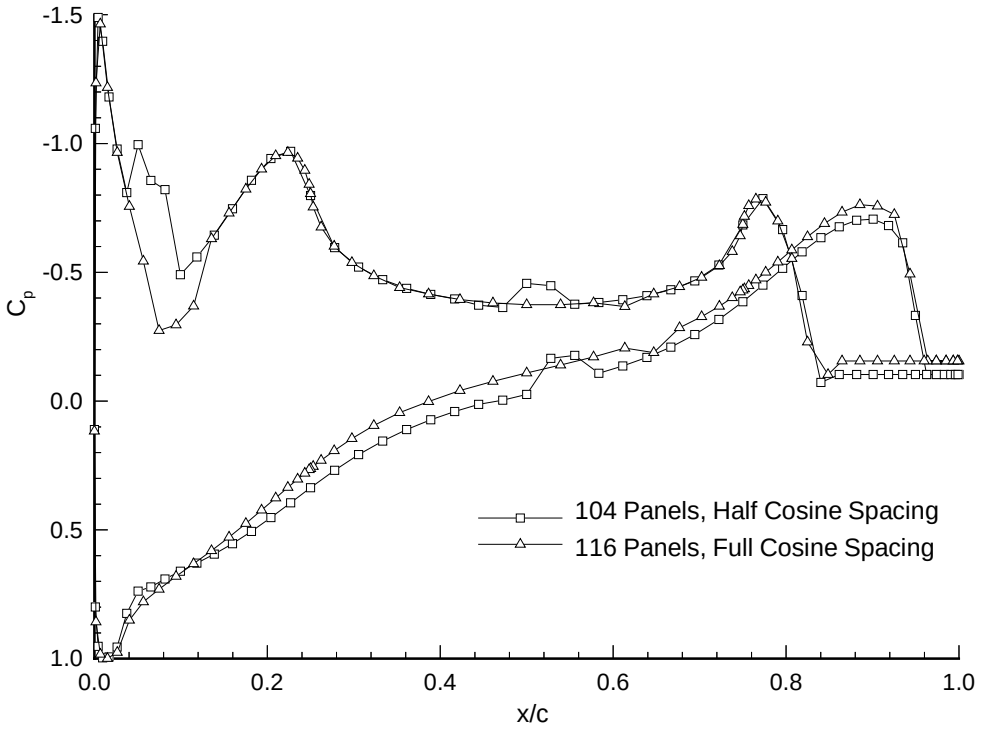

Figure 8.8: OPTCD2 Pressure Coefficient Predictions With and Without Panel Spacing Adjustments

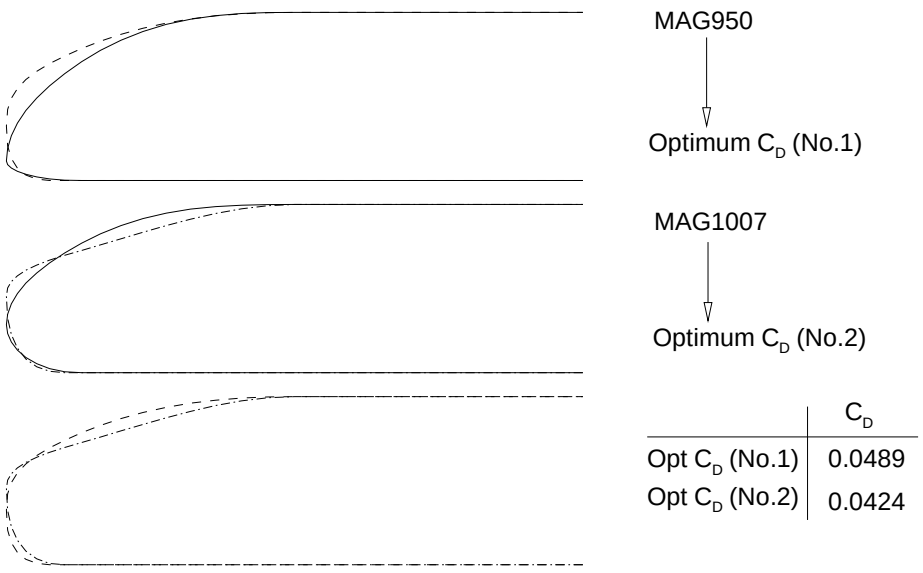

Figure 8.9: Comparison of Two Optimum Drag Coefficient Designs

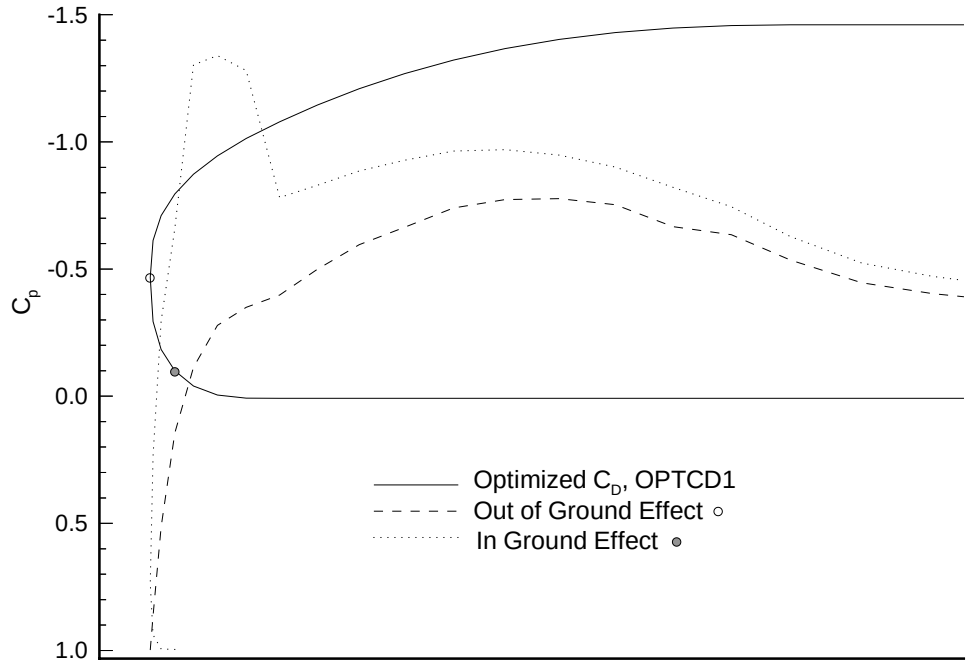

Figure 8.10: Leading Edge Suction Due to Ground Effect on Optimized Drag Coefficient Design, OPTCD1

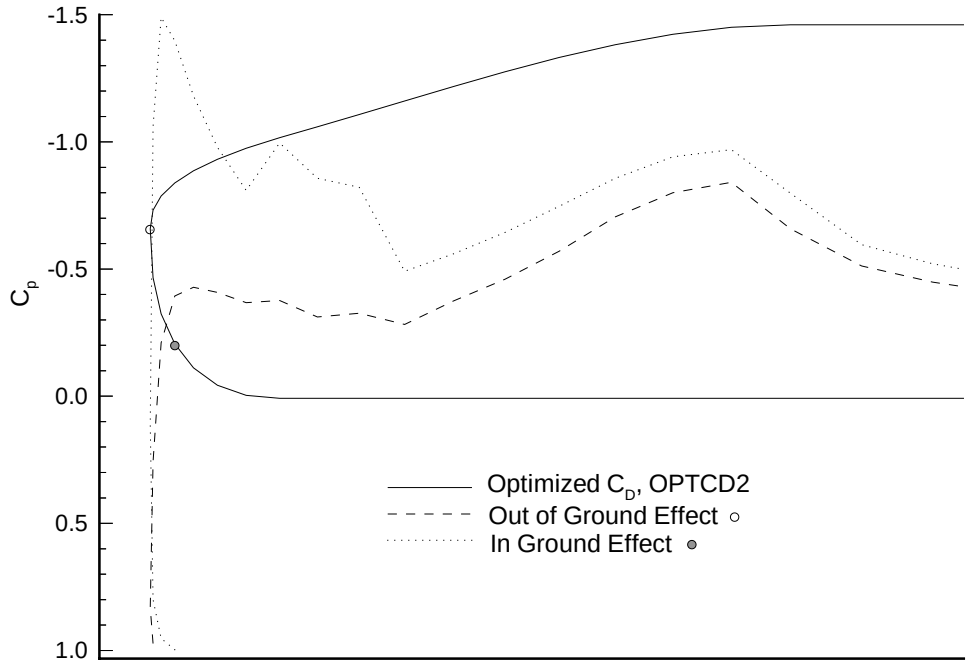

Figure 8.11: Leading Edge Suction Due to Ground Effect on Optimized Drag Coefficient Design, OPTCD2

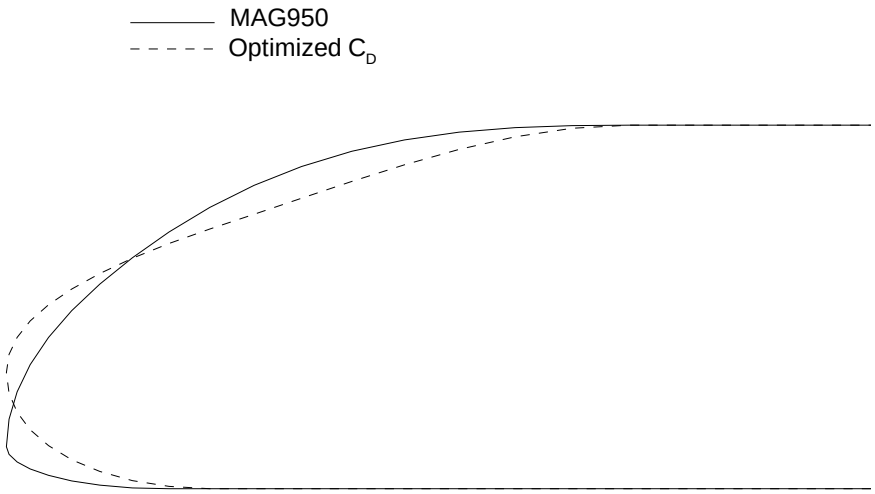

Figure 8.12: Optimum Drag Coefficient Design Using MAG950 Baseline for Out of Ground Effect Condition

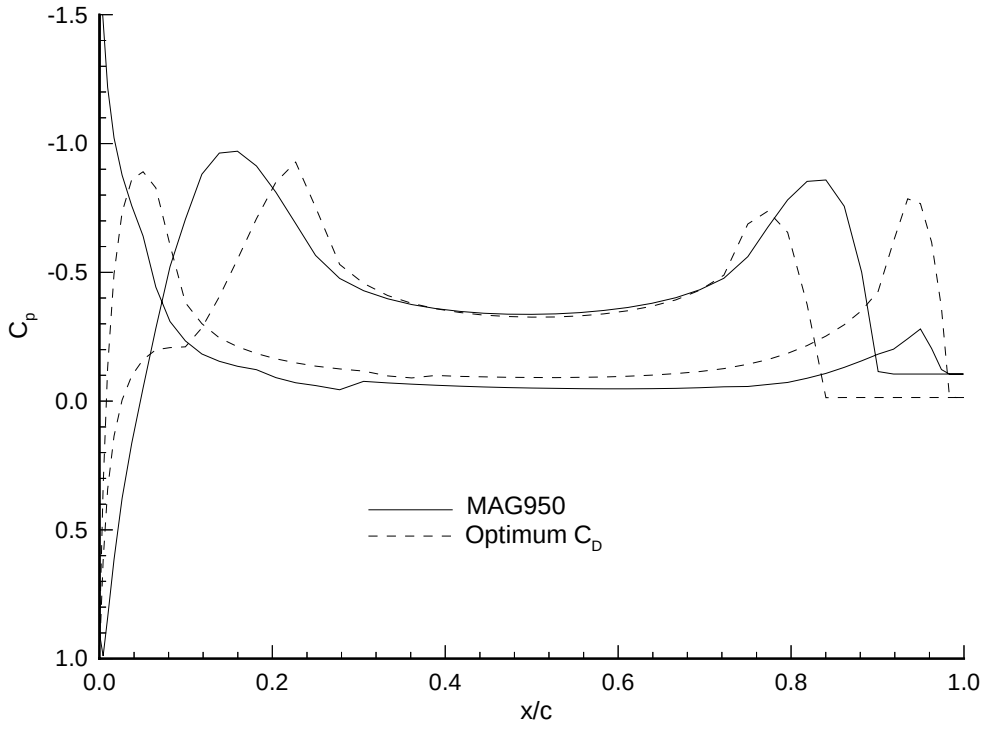

Figure 8.13: Pressure Coefficients for Optimum Drag Coefficient Design Operating Out of Ground Effect Compared to MAG950 Baseline

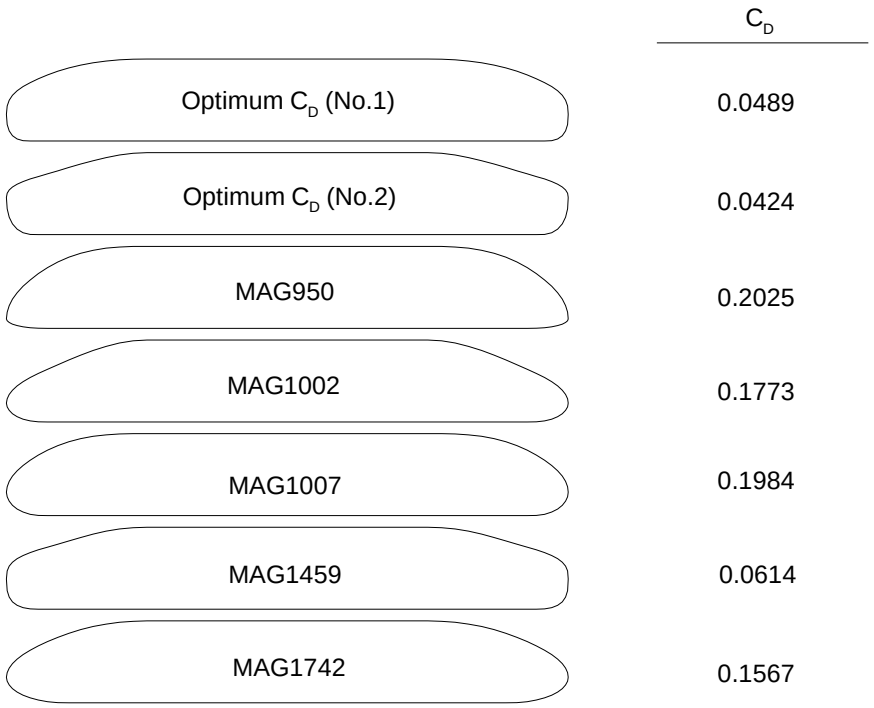

Figure 8.14: Optimized Drag Coefficient Designs vs. Northrop Grumman Designs

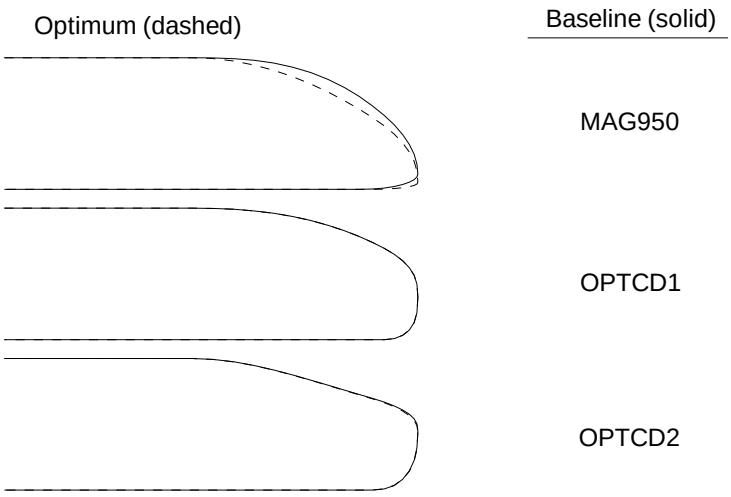

Figure 8.15: Maximum Lift to Drag Ratio Designs

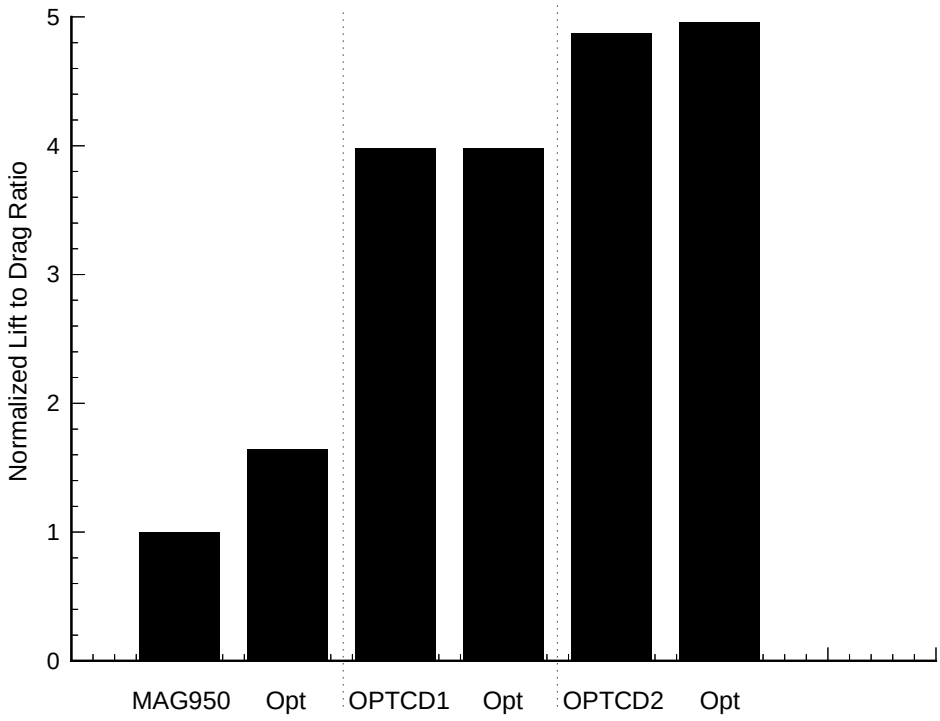

Figure 8.16: Comparison of Lift to Drag Ratio Designs

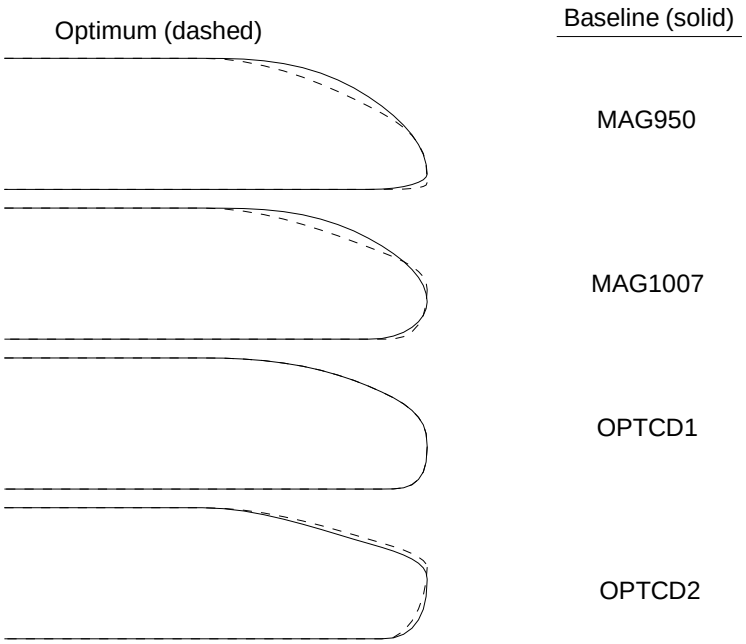

Figure 8.17: Minimum Operating Cost Designs

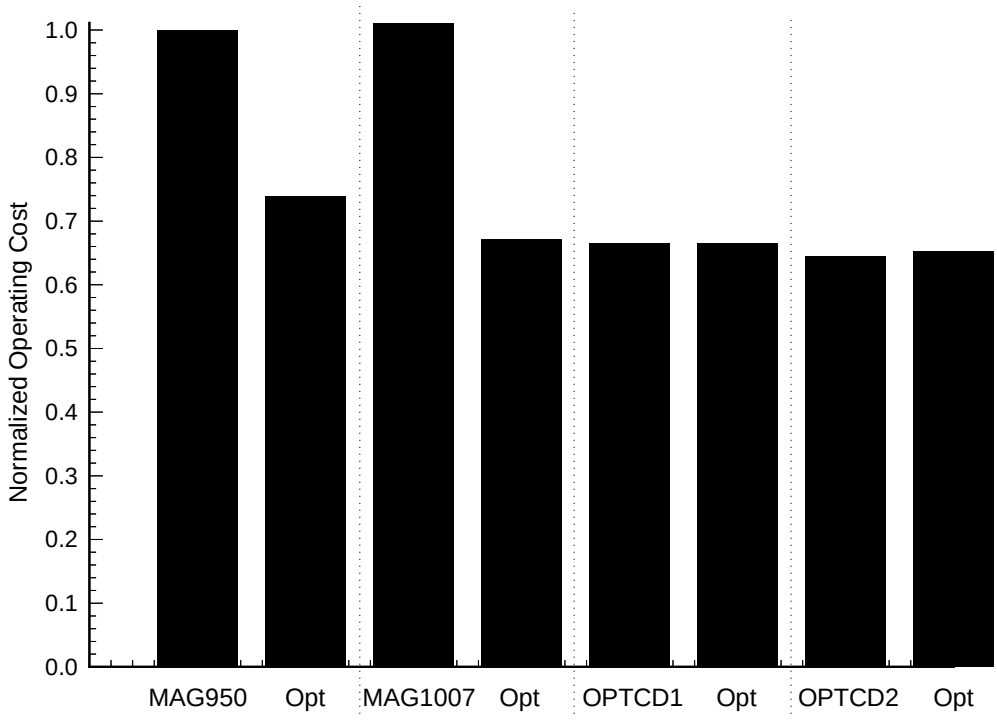

Figure 8.18: Comparison of Operating Cost Designs

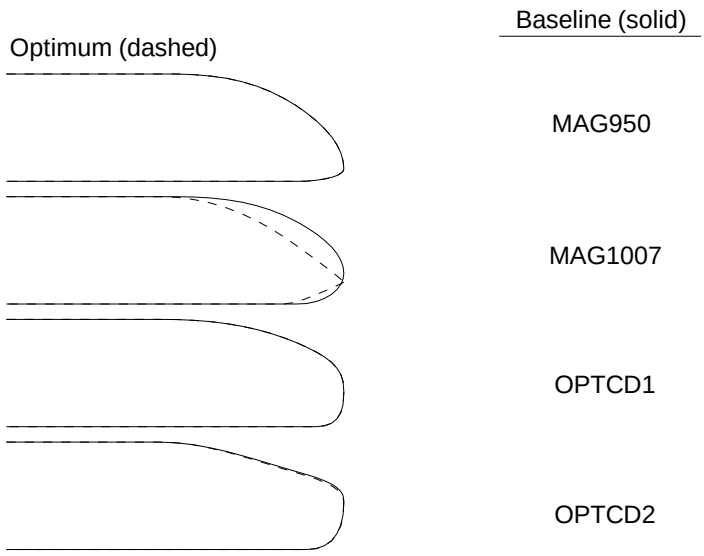

Figure 8.19: Minimum Acquisition Cost Designs

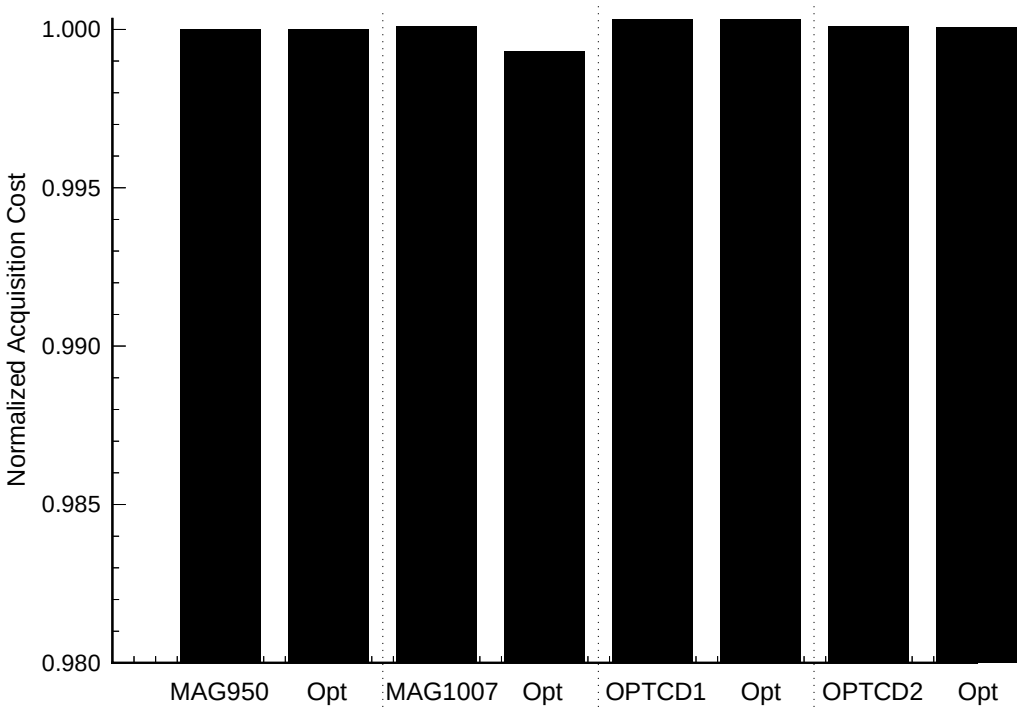

Figure 8.20: Comparison of Acquisition Cost Designs

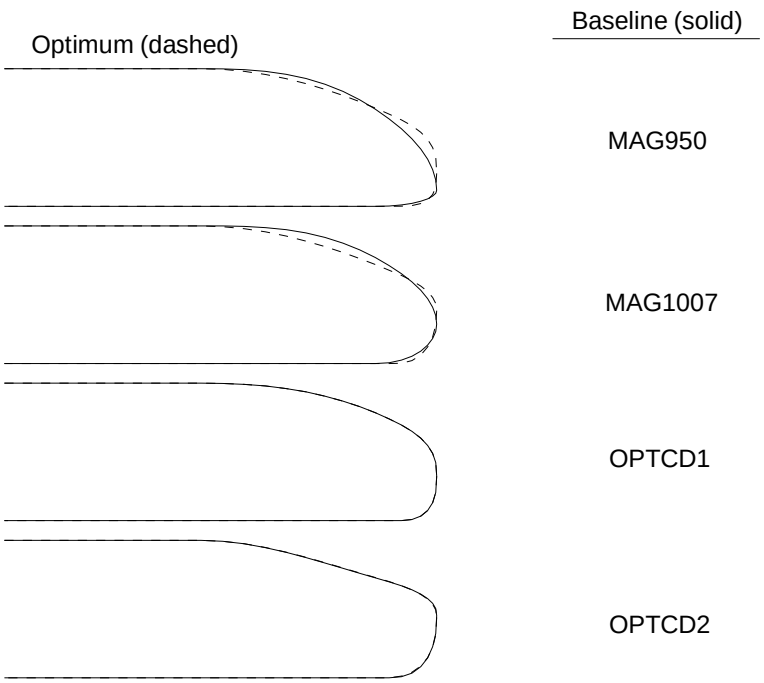

Figure 8.21: Minimum Life Cycle Cost Designs

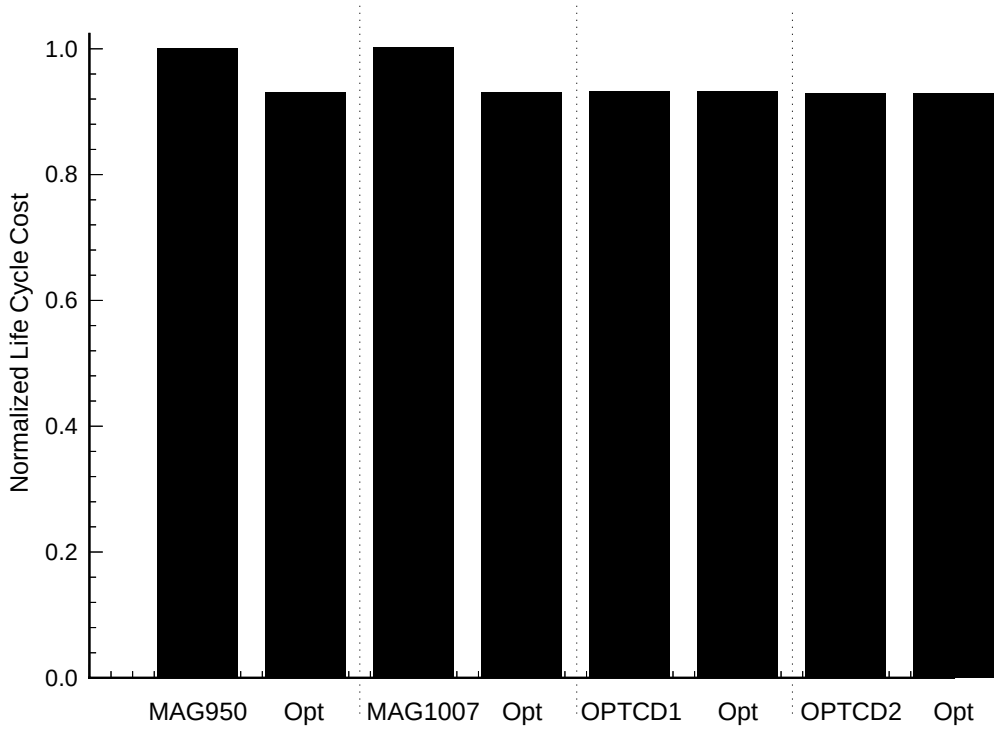

Figure 8.22: Comparison of Life Cycle Cost Designs

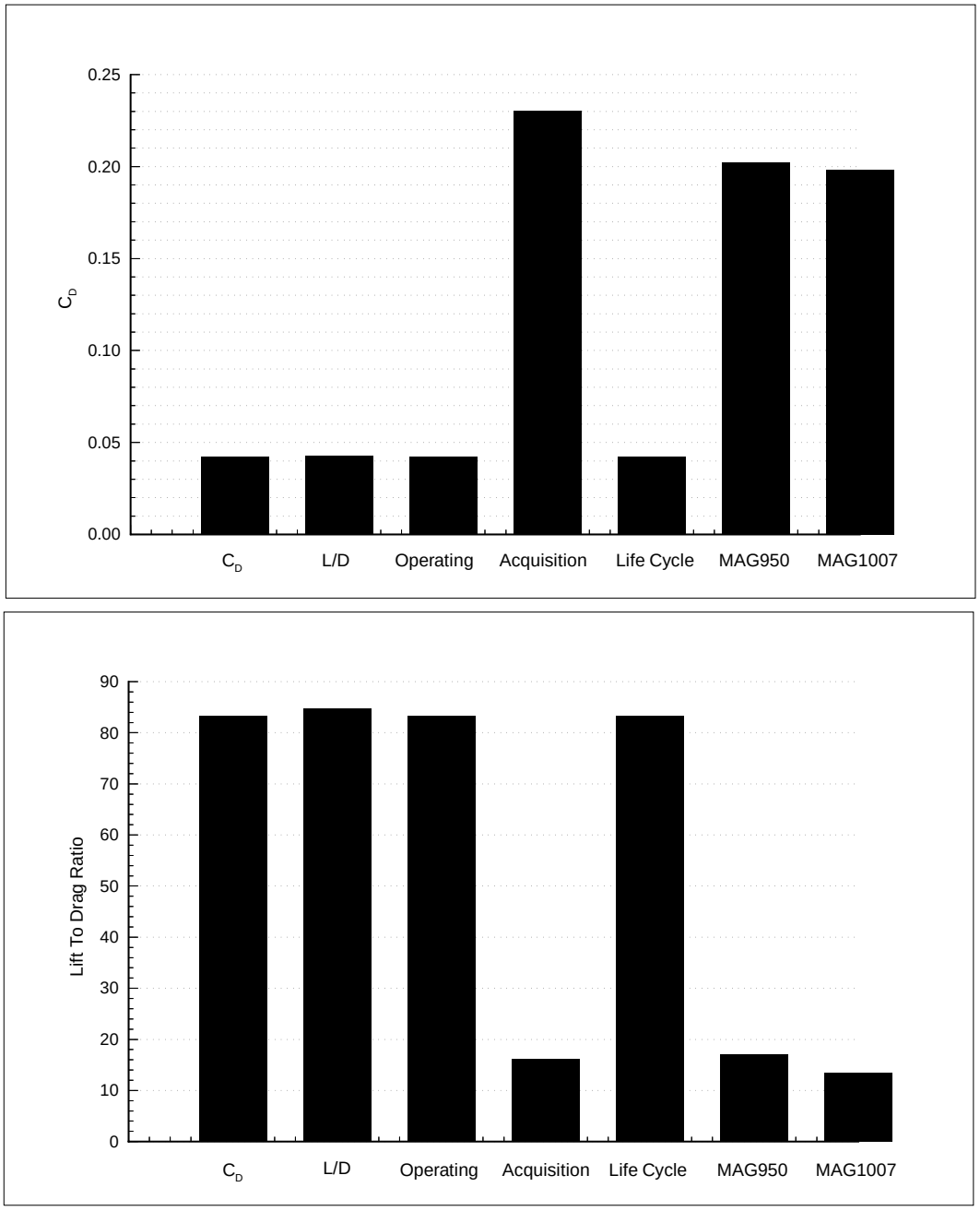

Figure 8.23: A Comparison of Drag Coefficient and Lift to Drag Ratio among Optimum Designs for Different Figures of Merit

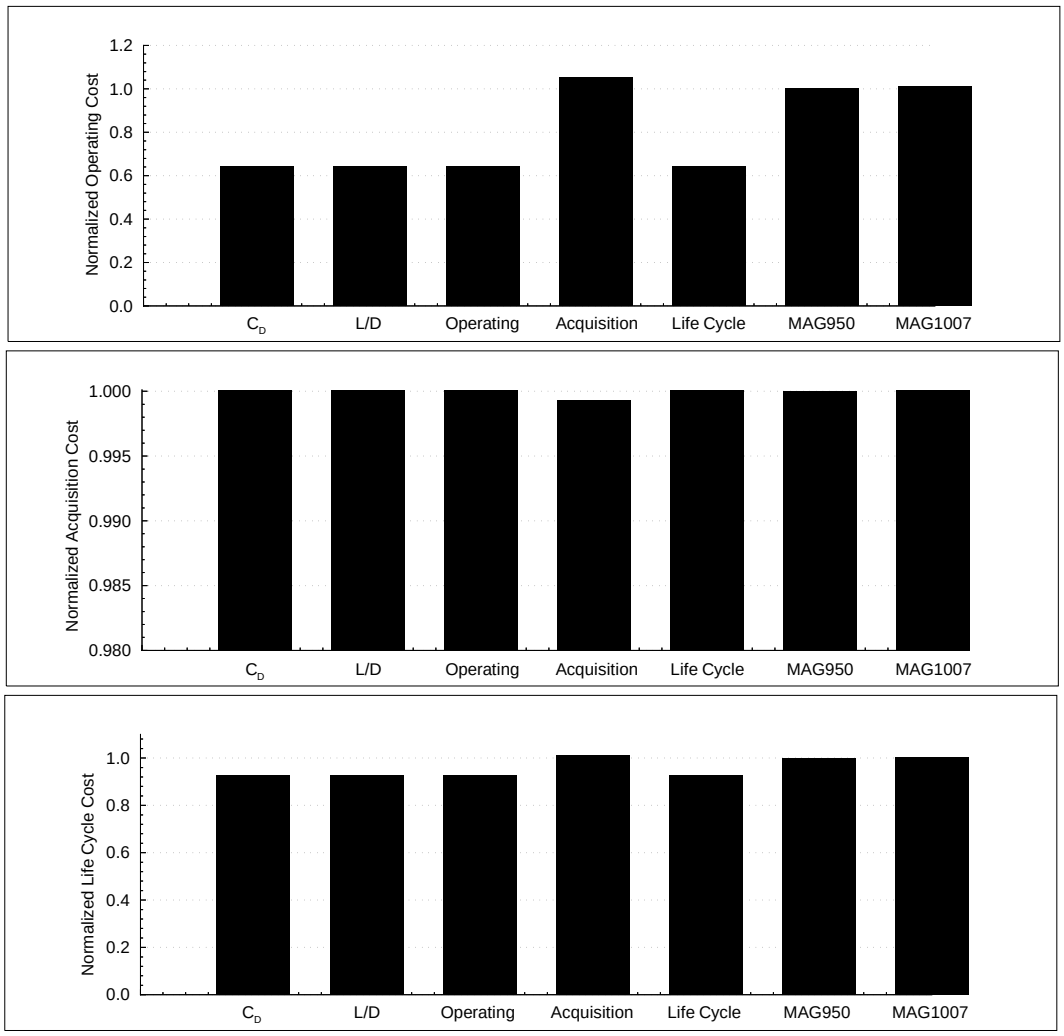

Figure 8.24: A Comparison of Operating Cost, Acquisition Cost, and Life Cycle Cost Among Optimum Designs for Different Figures of Merit

	C_D	L/D	DOC	Acq Cost	LCC	MAG950	MAG1007
XN	1.22	1.29	1.22	1.74	1.22	1.50	1.50
XF	1.61	1.63	1.61	1.78	1.61	1.50	1.50
θ	16.13	16.40	16.13	35.13	16.13	34.00	29.00
N	2.42	2.44	2.42	1.08	2.42	2.00	2.00
F	1.86	1.66	1.86	0.54	1.86	0.20	0.60

Table 8.1: Geometry Variables of Optimum Designs